

ORIGINAL ARTICLE

Influence of Pin Offset and Weave Pattern on the Performance of Al-Cu Joints Reinforced with Graphene Particles

M. Balasubramanian^{1*} and D. Jayabalakrishnan²¹Department of Mechanical Engineering, RMK. College of Engineering and Technology, Tiruvallur, India
Phone Number: +919841714830,²Department of Mechanical Engineering, Sriram Engineering College, Tamilnadu, India

ABSTRACT – The friction stir welding technique is currently employed for different alloy combinations like magnesium, titanium, copper, nickel-based composites. Dissimilar materials may be efficiently joined by the process and this has been used in several structural applications such as automotive components, aircraft structure, shipbuilding, and space shuttle external tank and train bodies. Even though improvement in the joint strength was achieved, problems such as voids, tunnels, cracks persisted in the weldments. The objective is to achieve defect-free joints. Tool pin offset for joining of aluminum alloy enables better stirring action and an easy flow of plasticised material in the weld nugget. Hence, to overcome the above-mentioned problem, a technique of combined effect of weaving, tool pin offset, and reinforcement of self-lubricated graphene nanoplatelets was attempted. The tensile strength obtained with the effect of tool rotational speed under weave weld with pin offset condition with reinforcement was 13.82 % higher than the weld obtained under the same condition without reinforcement. IMCs such as AlCu, Al₂Cu, and Al₄Cu₉ large size band layers were observed with the linear welding condition, whereas weave welding conditions resulted in the formation of the thin uniform layer.

ARTICLE HISTORYRevised: 6th Sept 2020Accepted: 22nd Sept 2020**KEYWORDS***FSW; Graphene; Weaving; Pin offset; Mechanical properties; Wear*

INTRODUCTION

Friction stir welding (FSW) is additionally an eco-friendly method due to the smaller energy consumption throughout this process, and the tool is non-consumable avoiding the necessity of filler material. FSW finds a wide range of applications in aerospace, automotive, naval industries for the last two decades owing to good machinability, high strength with lesser weight and corrosion resistance properties. Friction stir welding of AA6061-T6 plates with a new tool-path movement was proved by Jayabalakrishnan and Balasubramanian [1] that the tensile strength of the joints was remarkably influenced by the tool-path pattern. Welding of thin sheets was accomplished by Jayabalakrishnan and Balasubramanian [2] between Al and Cu with novel joint geometry through form clamping and chemical diffusion bonding. Ouyang et al. [3] identified a mechanically mixed region of various IMCs like CuAl, CuAl₂, and Cu₉Al₄ along with α -Al was present which resulted in the lower dissolution of Cu in Al despite the high solubility of Al in Cu. Liu et al. [4] observed a better welding strength of 296 MPa due to the existence of a mixed structure on the Al side of the stir zone and the lamellar arrangement on the Cu side of the stir zone.

Previous experience reveals difficulties faced during the joining of Al to Cu. Linear motion of the tool profile caused tunnel defects and voids due to improper stirring time was discovered by Sinha et al. [5]. According to Yuqing et al. [6], tool pin offset for joining of thick plates of aluminium alloy reported better stirring action and an easy flow of plasticised material in the weld nugget. Cabibbo et al. [7] studied the effect of pin rotation around its axis is normal to the weld line and identified that the translation of the pin along the axis would overcome the formation of the oxide layer and avoids a severe weld defect.

Mehta and Badheka [8] found that defect-free dissimilar Cu-Al friction stir welded joints were achieved using tool tilt angles of 2°, 3°, and 4°. The highest tensile strength and hardness observed at 4° tilt angle was 117 MPa and 181 HV respectively in the nugget zone. Mehta and Badheka [9] found that the quantity of IMC phases formed in SZ increased by the expansion of preheating current. The development of IMC experienced a big reduction as a cooling effect from compressed air to water increased. The maximum hardness of stir zone was identified for both hybrid FSW process strategies concerning ordinary FSW. Galvao et al. [10] revealed that there was a formation of AlCu IMCs compound at the Al side of the weld nugget, and Cu₉Al₄, Al₂Cu at the Cu region.

Selamat et al. [11] performed FSW on AA5083-AA5083 and AA5083-AA6061 with a threaded tool resulted in the formation of onion ring and wavy distortion in the nugget zone. The efficiency of joint AA6061-AA5083 was 93% and

34% compared to AA6061 and AA5083, respectively. Shah et al [12] identified that tool offset plays a major role in on the microstructural and mechanical properties of thick-plate 5052-6061 dissimilar weld joint. Ibrahim Sabry and El-Kassas et al. [13] noted that the percentage of SiC_p aluminium matrix composite differs from the manufactured alloy matrix and aluminum matrix composite to comprehend the impact of rotational speed, travel velocity and Sic particle on FSW. Elongation (%) came down in welded joint due to the disintegration of SiC_p reinforcing agents and development of fine grains structure in the weld zone following to FS welding. Sathari et al. [14] studied the FSW of 2.0 mm thick plates of AA7075 and AA6061. Maximum tensile strength value of 207 MPa was obtained on the advancing side of AA6061, compared to AA7075 positioned on the advancing side with a minimum tensile strength of 160 MPa due to severe tunnel defects inside the weldment and surface galling that contribute to failure.

Even though improvement in the joint strength is evident from literature, various problems such as voids, tunnels, cracks, and improper stirring time were seen. Tool pin offset is reported to provide better stirring action and an easier flow of plasticised material in the weld nugget. Hence, to overcome the above-mentioned problem, the present investigation has proposed a novel technique, with a combined effect of weaving, tool pin offset, and addition of self-lubricated graphene nanoplatelets as a reinforcement material.

MATERIALS AND METHODS

The base materials used in this study were aluminium alloy (AA 6601-T6) and pure copper with dimensions of 100 mm length, 50 mm width, and 6 mm thickness. The graphene nanoplatelets (GNPs) having a surface area of 500 m²/g, a molecular weight of 12.01 g/mol, an average density of 0.3 g/cm³, and size of 25µm, were used for the present study. The welding parameters and their ranges are shown in Table 1. Based on the trial experimental results obtained and the visual inspection of the joint for surface quality, the following experiments were performed. Weave welding is a type of friction stir welding method in which the tool is moved eccentrically in a weaving pattern. The eccentric motion is governed by the welding speed.

Table 1. Important parameters.

S. No	Factors	Unit	Range
1	Tool rotational speed (N)	rpm	800-1600
2	Welding speed (v)	mm/min	30-70
3	Axial load (F)	kN	8-16

An elliptical groove was made along the length of the weld line to fill the graphene particles. A total volume of 2.06% graphene particles was used as a reinforcement material. This ellipsoidal groove ensured the restriction of the spilling of graphene particles during the stirring process. The tool path was governed by the elliptical motion given by Eq. (1);

$$\text{Per} = 2\pi \sqrt{\frac{1}{2}(a^2 + b^2)} \quad (1)$$

Where a is the width of the bead, and b is the tool return distance to the linear axis. The tool takes two times of stirring with the linear weld. Hence the elliptical path would be governed to the linear axis by the following Eq. (2). The following experiments were conducted as depicted in Figure 1.

- i. Linear weld without pin offset (LW-WOPO)
- ii. Linear weld with pin offset (LW-WPO)
- iii. Weave weld (eccentric) without pin offset (WW-WOPO)
- iv. Weave weld (eccentric) with pin offset (WW-WPO)

The tensile strength of the specimens was tested using 40 tonnes capacity universal testing machine (MTS C44, India) as per ASTM E 8 at an of strain rate of 1x10⁻³ m/s. The impact strength of the welded samples was tested using 30 J capacity impact tester (Kristal, India) as per ASTM E 23 at a pendulum velocity of 5.23 m / sec. Vickers micro-hardness testing machine (Make: Zwick and Model: 3212) was employed for measuring hardness with load 100 g and dwell time 15 sec. The specimen geometry for testing is represented in Figure 2. Evaluation of the microstructure of the welded portion was carried out by utilising an optical microscope with 25× lens zooming capacity.

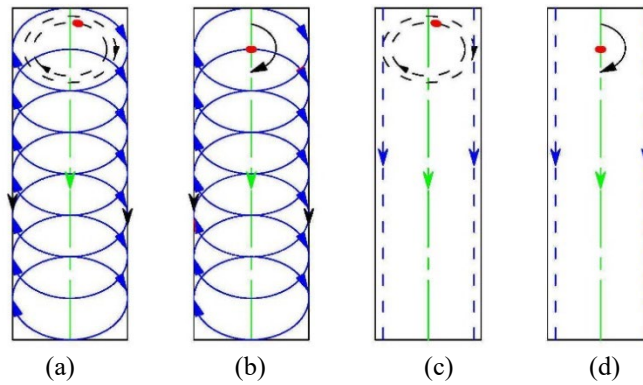


Figure 1. (a) Weave weld with pin offset, (b) weave weld without pin offset, (c) linear weld with pin offset and (d) linear weld without pin offset

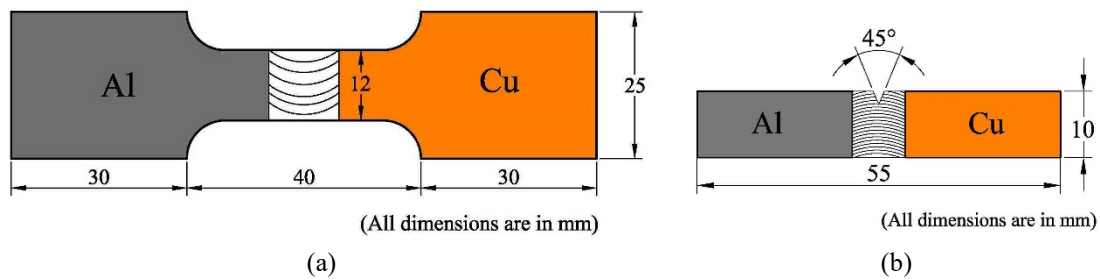


Figure 2. Dimensions of (a) tensile and (b) impact specimen

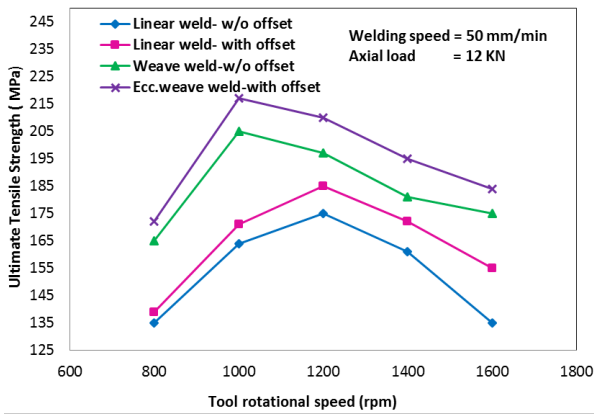
RESULTS AND DISCUSSION

Effect of Tool Rotational Speed on Mechanical Properties

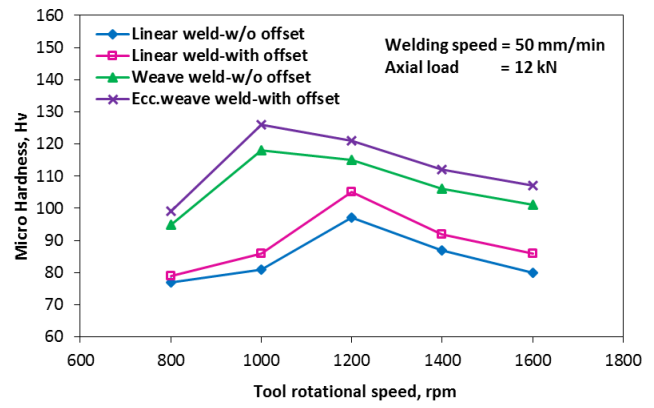
The impact of varying rotational speed of the tool on the tensile properties of the joints at a constant welding speed of 50 mm/min and an axial load of 12 kN was studied. Effect of tool rotational speed in the linear weld and weave weld without and with tool pin offset condition for the ultimate tensile strength is presented in Figure 3(a). An earlier study revealed a maximum UTS of 130 MPa in friction stir welding (FSW) of dissimilar Al- pure Cu [5]. Effect of tool rotational speed in the linear weld and weave weld without and with tool pin offset condition for the microhardness is presented in Figure 3(b). It was reported by Li et al. [15] that a maximum hardness of 110 HV was reported in FSW of dissimilar Al-pure Cu. Effect of tool rotational speed in the linear weld and weave weld without and with tool pin offset condition for the yield strength is presented in Figure 3(c). The current investigation yielded the best yield strength of 182 MPa through weave weld with pin offset condition is found to be better than the yield strength of 118.95 MPa obtained by Sahu et al. [16]. Effect of tool rotational speed in the linear weld and weave weld without and with tool pin offset condition for the impact strength is presented in Figure 3(d). Effect of tool rotational speed in the linear weld and weave weld without and with tool pin offset condition for the ultimate tensile strength is presented in Figure 3(e). A maximum of 10 % elongation was reported by Kahl et al. [17] in FSW of dissimilar Al-Cu. The results are tabulated and presented in Table 2.

Table 2. The effect of tool rotational speed on mechanical properties.

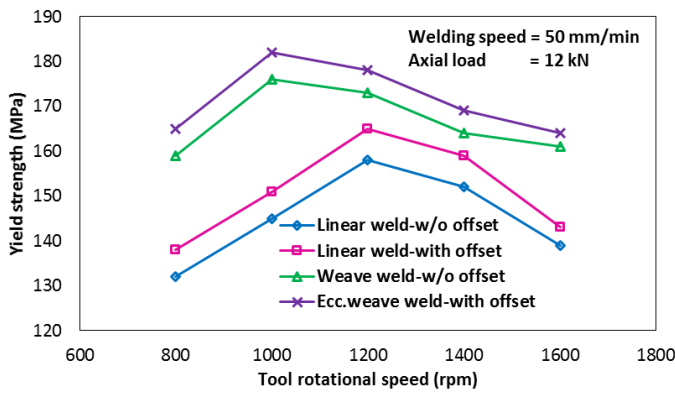
Type of welding	Ultimate tensile strength (MPa)	Yield strength (MPa)	Elongation (%)	Impact (J)	Microhardness (HV)
Linear weld without pin offset	175	158	11.3	9.4	97
Linear weld with pin offset	185	165	10.7	10.2	105
Weave weld without pin offset	205	176	9.7	11.6	118
Weave weld with pin offset	225	182	9.4	12.4	126



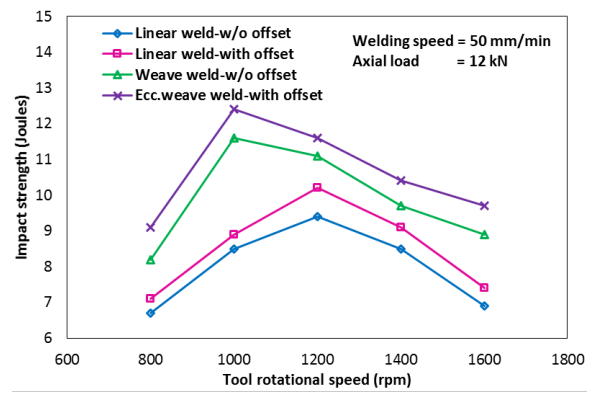
(a) tool rotational speed vs tensile strength



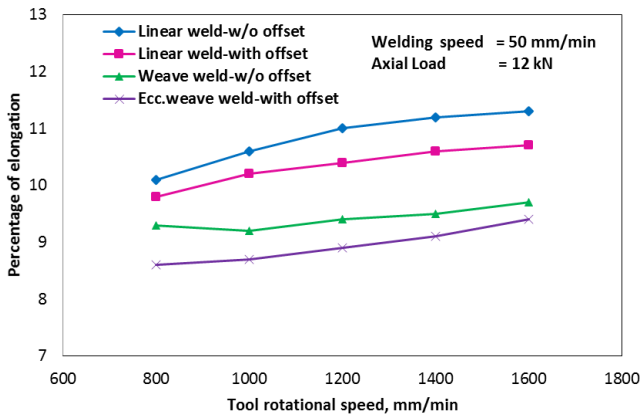
(b) tool rotational speed vs hardness



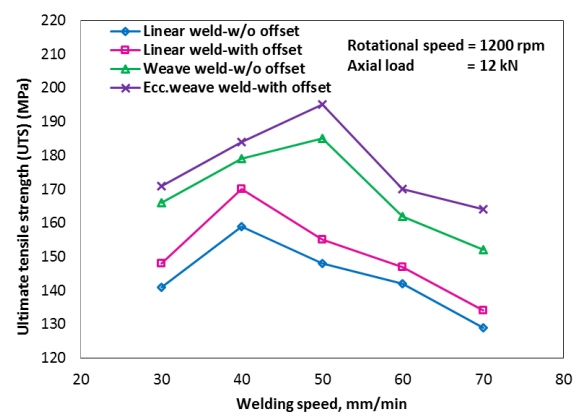
(c) tool rotational speed vs yield strength



(d) tool rotational speed vs impact strength



(e) tool rotational speed vs elongation



(f) welding speed vs tensile strength

Figure 3. Effect of tool rotational speed and welding speed on mechanical properties.

Effect of Welding Speed on Mechanical Properties

Joints fabricated under varying welding speed for linear weld and weave weld without pin offset condition for the ultimate tensile strength is presented in Figure 3(f). Earlier studies by Bhattacharya et al. [18] achieved maximum UTS of 135 MPa. Joints fabricated under varying welding speed for linear weld and weave weld without pin offset condition for the microhardness is presented in Figure 4(a). The impact of welding speed on yield strength concerning linear weld and weave weld without pin offset is shown in Figure 4(b). Figure 4(c) depicts the effect of welding speed for linear and weave weld without pin offset condition for the impact strength. The impact of welding speed on percentage elongation for linear and weave weld without pin offset condition is shown in Figure 4(d). Previous studies by Sahu et al. [19] achieved a maximum elongation of 8.6 % in FSW of dissimilar Al-Cu. The results are tabulated and presented in Table 3.

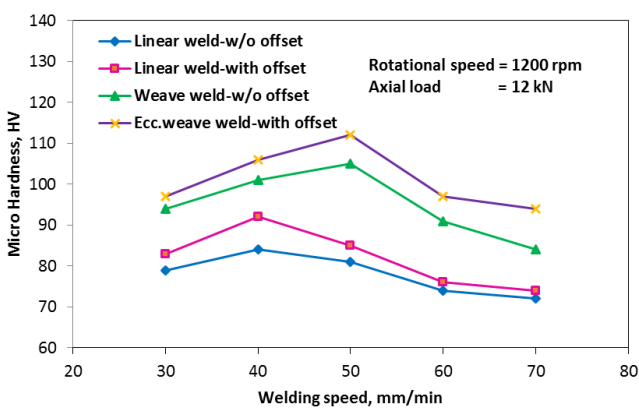
Table 3. The effect of welding speed on mechanical properties.

Type of Welding	Ultimate tensile strength (MPa)	Yield strength (MPa)	Elongation (%)	Impact (J)	Microhardness (HV)
Linear weld without pin offset	159	138	9.6	7.2	84
Linear weld with pin offset	170	146	8.8	8.1	92
Weave weld without pin offset	184	158	8.0	9.1	105
Weave weld with pin offset	195	164	7.6	10.2	112

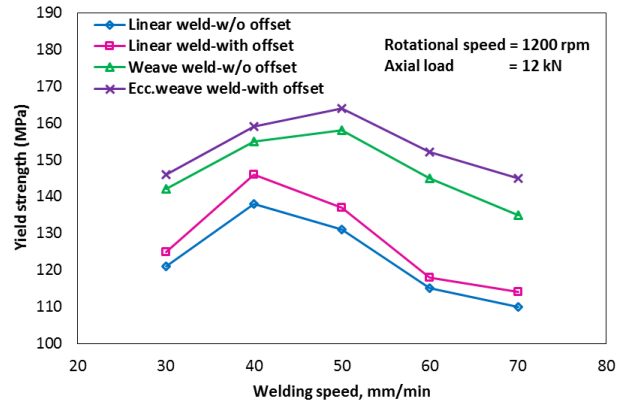
Effect of Axial Load on the Mechanical Properties

Figure 4(e) shows the influence of an axial load on UTS, under linear and weave weld with and without pin offset condition. A maximum of 208 MPa in FSW of dissimilar Al-Cu was achieved by Akinlabi [20]. The effect of varying an axial load on the microhardness of the Al-Cu joints is shown in Figure 4(f). It was reported by Singh et al. [21] that with an increase in axial load, the pin plunged deep inside the material creating a high shear force that dragged the phase materials shifting towards the advancing side.

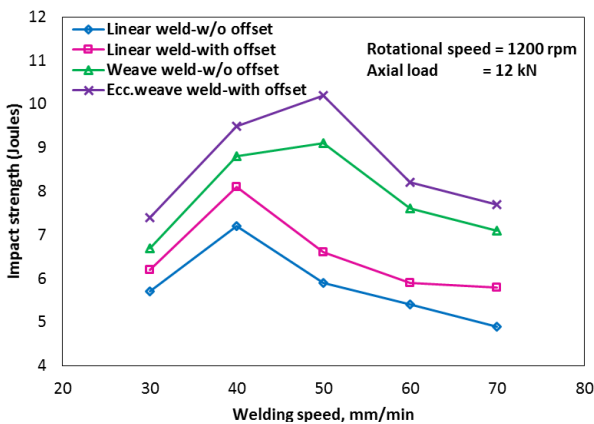
The impact of an axial load on the yield strength of the Al-Cu joints is shown in Figure 5(a). An earlier study by Sahu et al. [19] achieved a maximum yield strength of 119.3 MPa. Figure 5(b) shows the influence of the axial load on the impact strength of the Al-Cu joints. The impact of varying the axial load on the percentage of elongation of the Al-Cu joints is shown in Figure 5(c). Maximum elongation of 3 % was observed by Avettand-Fenoel et al. [22] in joining of dissimilar Al-Cu. The results are tabulated and presented in Table 4.



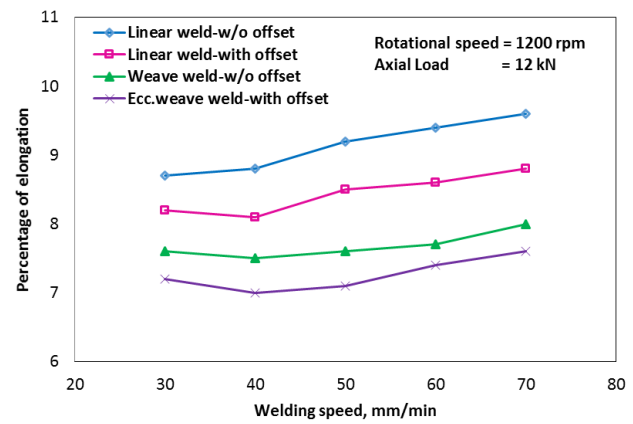
(a) welding speed vs microhardness



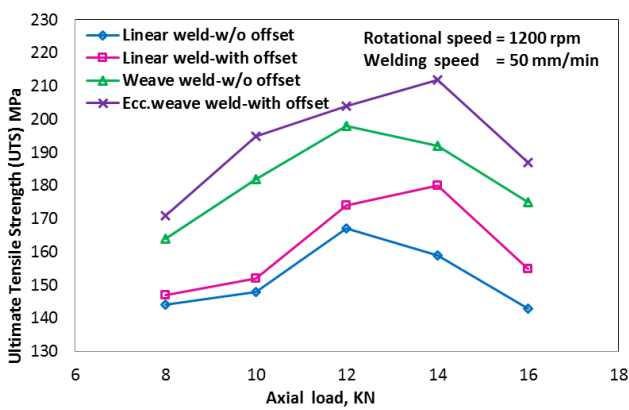
(b) welding speed vs yield strength



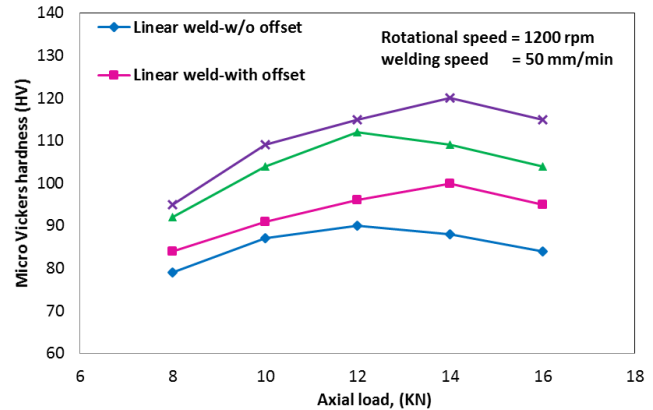
(c) welding speed vs impact strength



(d) welding speed vs elongation



(e) axial load vs tensile strength

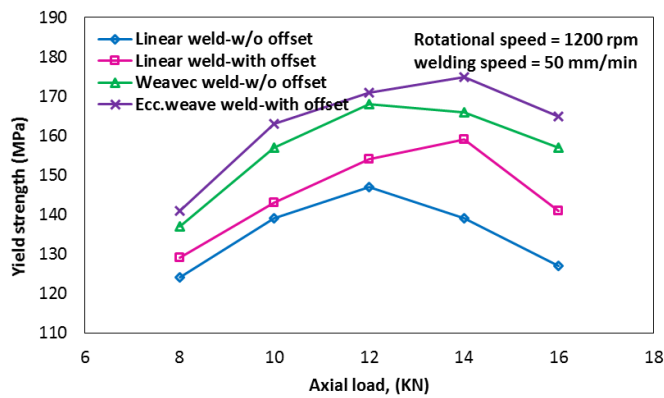


(f) axial load vs micro hardness

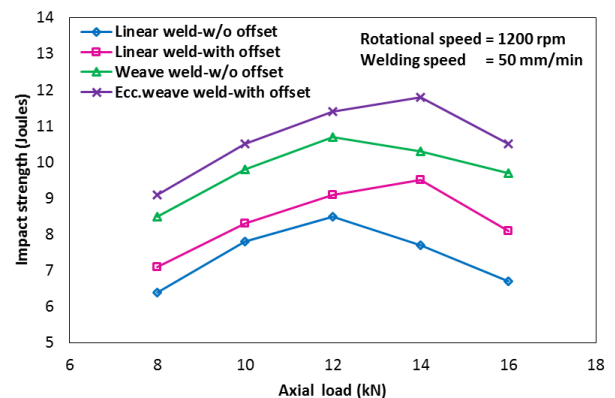
Figure 4. Effect of welding speed and axial load on mechanical properties.

Table 4. The effect of axial load on the mechanical properties.

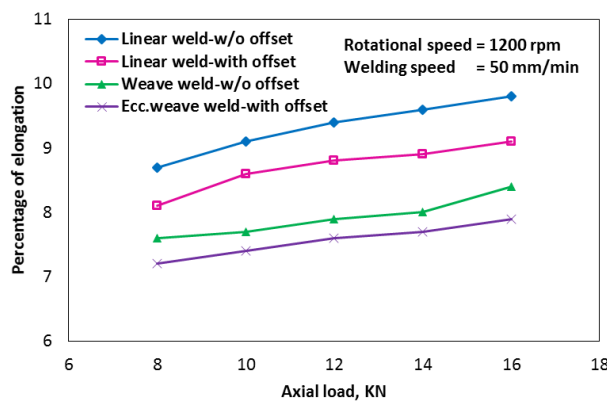
Type of welding	Ultimate tensile strength (MPa)	Yield strength (MPa)	Elongation (%)	Impact (J)	Microhardness (HV)
Linear weld without pin offset	167	147	9.8	8.5	90
Linear weld with pin offset	180	159	9.1	9.5	100
Weave weld without pin offset	198	168	8.4	10.7	112
Weave weld with pin offset	212	175	7.9	11.8	120



(a) axial load vs yield strength



(b) axial load vs impact strength



(c) axial load vs elongation

Figure 5. Effect of axial load on mechanical properties at the welding speed of 50 mm/min.

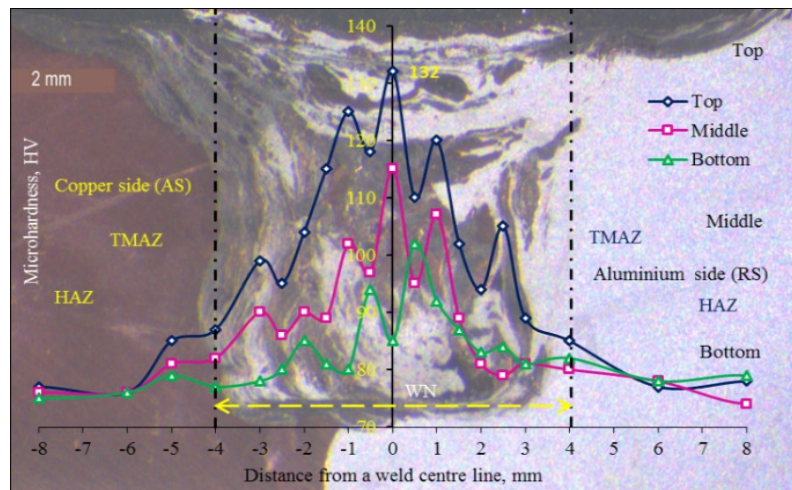


Figure 6. Microhardness along the transverse cross-section of the weld made by WW-WPO (with GNPs) at 1000 rpm; 50 mm/min; 12 kN.

Effect of Process Parameters on Mechanical Properties

It was noticed from the observed results that the addition of graphene nanoplatelets increased the hardness significantly without loss of ductility on Al-Cu in the FSW joint. The transverse cross-section of the weld joint under weave weld condition along the top, middle, and bottom of the nugget region is shown in Figure 6. It is observed from Figure 6 that the top of the weld nugget showed a higher hardness of 132 HV compared with the middle and bottom layers of the nugget. This is due to the grain refinement and higher dislocation density at the nugget. The HAZ showed a minimum hardness of 76 HV compared with the other zones of joint, as shown in Figure 6. In FSW dissimilar welding, the higher hardness was recorded at the Al-Cu weld nugget because of the dynamic recrystallisation. In general, an increase in tool rotational speed increases the grain refinement strengthening, which are the reasons for an increase in the hardness in SZ. The high fluctuation in the hardness within the nugget is due to the existence of corresponding IMCs, which can be confirmed with X-ray diffraction analysis (XRD) results, as shown in Figure 7. The structural revelation of as-deposited Al_2Cu was examined through an X-ray diffraction measurement.

Figure 7 shows the XRD patterns of graphene doped Al_2Cu thin films. All the XRD peaks are found indexed into the diffraction pattern of triclinic structure. Along with corresponding (hkl) values of intense diffraction planes are (211), (002), (12), and (402) observed with JCPDS card no. 89-1980. The XRD spectrum shows the diffraction peaks with a slight shift to the higher direction detected at concentrations of graphene with samples, respectively. This indicates an increase in the average lattice imperfection increase with graphene doping, which could be due to the presence of graphene into the Al sites and the subsequent deformation of Al_2Cu lattice.

The weave weld with pin offset provides a defect-free weld joint as shown in Figure 8(a) the rotational tool speed of 1000 rpm is high enough for the accomplishment of a stable joint. Deficient temperature contribution at low tool rotational speed of 800 rpm prompting to the low quality of weld as seen in Figure 8(b). This was also found by Singarapu et al. [23]. The homogenous mixing of Cu particles in the AA 6061-T6 matrix was attained in weave weld condition with the use of GNPs due to a larger stirring area and a high volume of material transportation. The creation of hard IMCs, as well as the strong plastic deformation in the SZ, led to increasing the hardness which was due to the grain refinement as per the Hall-Petch effect. The increase in the hardness of 132 HV at the top of the weld nugget was due to the presence of a high amount of disintegration of Cu particles that might be regulated by selecting appropriate process parameters and the addition of graphene strengthened the weldments. Jayabalakrishnan and Balasubramanian [24] revealed that on eccentric stirring with tool pin offset produced minimal wear of 5 μm . Defects on the weldments prove the existence of fragmental cracks in eccentric welding.

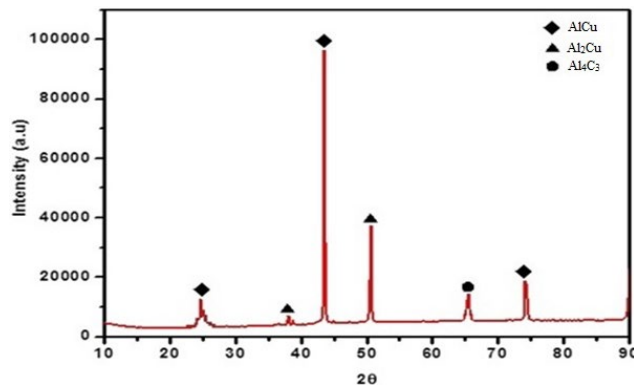


Figure 7. X-ray diffraction pattern of WW-WPO (with GNPs).



Figure 8. Surface morphology of AL-Cu joint fabricated at 1000 rpm under EWW-WPO (with GNPs) at (a) 1000 rpm and, (b) 800 rpm.

The microstructure of the base metal of AA6061 and pure copper is shown in Figure 9(a)-9(b). The optical microscope (OM) images justified a grain microstructure refinement in the SZ of the weld joints. The spread of copper particles in the aluminium matrix in the form of vortex flow at the top surface of the nugget could be observed through OM, as shown in Figure 9(c). The formation of a long band of copper metal over the aluminium phase could be seen in Figure 9(d). The onion ring formation is shown in Figure 9(e) is the direct evidence for material transportation in the FSW. With the effect of tool rotational speed of 1000 rpm, the nanoplatelets are evenly dispersed throughout the weld nugget and fill the voids resulting in the absence of defects in the joint as shown in Figure 10.

Figure 11(a) justifies that the tool rotational speed of 1600 rpm resulting in the improper mixing at the interface zone and intensive material clustering existence at the SZ owing to the improper material flow caused by the tool shoulder. The aggregation of materials occurred closer to the thermomechanically affected zone (TMAZ) due to the downward movement of the materials formed by the pin. EDAX was carried out in the dark and bright region of location L1, where the Cu and GNPs were present in the Al matrix at the stir zone and also confirmed the existence of a different layer of IMCs. With the addition of GNPs for the condition of WW-WPO, similar proportions of Al and Cu phases presence in SZ (C - 10.37 %; Al - 39.73 %; Cu - 37.36 %) were identified and presented in Figure 10. The EDAX revealed the existence of GNPs through the %C present. The overall Al and Cu particles dissipated in the NZ were found to vary from point to point. This was due to the formation of different IMCs. There are various IMCs, namely AlCu, Al₂Cu, Al₄C₃ identified the from atomic weight percentage in the SZ for different welding conditions. The formation of IMCs was further confirmed through XRD analysis.

Under the weave weld, the stirring process was more efficient through stirring larger areas. So, the observed results confirmed WW-WPO providing adequate heat input and thereby increasing UTS compared with the other three welding conditions. In the weave weld with tool offset condition and GNP's, the size of the stir zone increased due to the weave pattern of tool movement and subjected to intensive plastic deformation. The effect of the self-lubricating nature of carbonaceous nano platelets resulted in the formation of a recrystallised equiaxed fine-grained microstructure, as shown in Figure 10. This could avoid the fragmental cracks and increase the tensile strength by utilising weave weld with tool pin offset. Hence, in our investigation at 1000 rpm, the highest tensile strength of 217 MPa was attained in weave weld with pin offset at a nominal welding speed of 50 mm/min using GNPs reinforcement. Previous literature in FSW of dissimilar AA6061-pure Cu reported the maximum tensile strength of 158 MPa [25], 170 MPa [26], and 135 MPa [18].

The experiments revealed that the increase in heat input leading to the formation dissolution and coarsening of strengthening precipitates at the stir zone (SZ) and the YS of the FSW joints led to reducing by lowering of dislocation density. The addition of nanoplatelets and active stirring effect by the tool in the weld nugget under weave weld condition increased the dispersion of nanoplatelets which can be observed in Figure 10. These GNPs acted as fibroid particles to hold the ductile bondage in increasing the yield strength. This leads to a maximum yield strength of 182 MPa with the tool rotational speed of 1000 rpm.

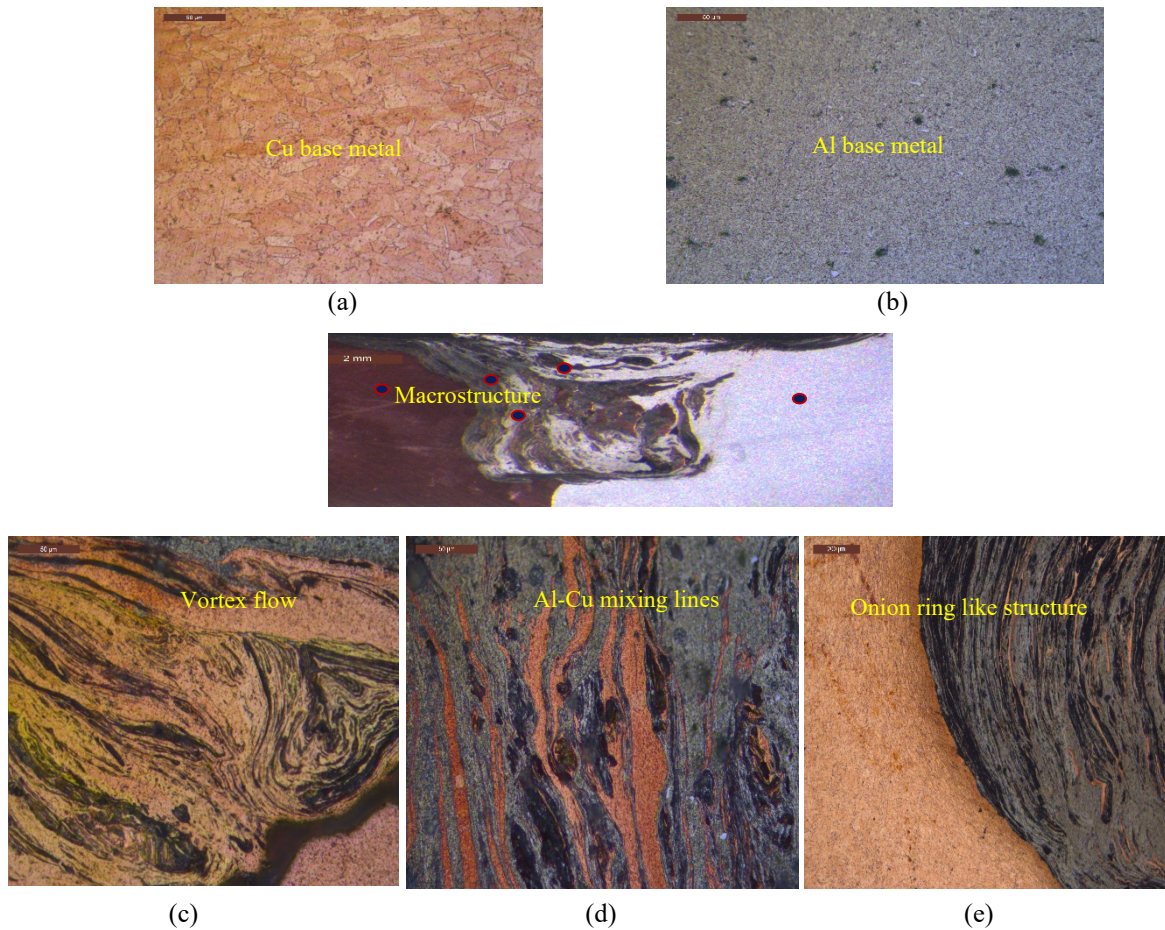


Figure 9. Macrostructure of joint made by WW-WPO (with GNPs) of 1000 rpm (a) Cu base metal, (b) Al base metal, (c) vortex flow like intercalated pattern, (d) lamellar like shear bands in the weld region (mixing lines) and, (e) onion ring structure.

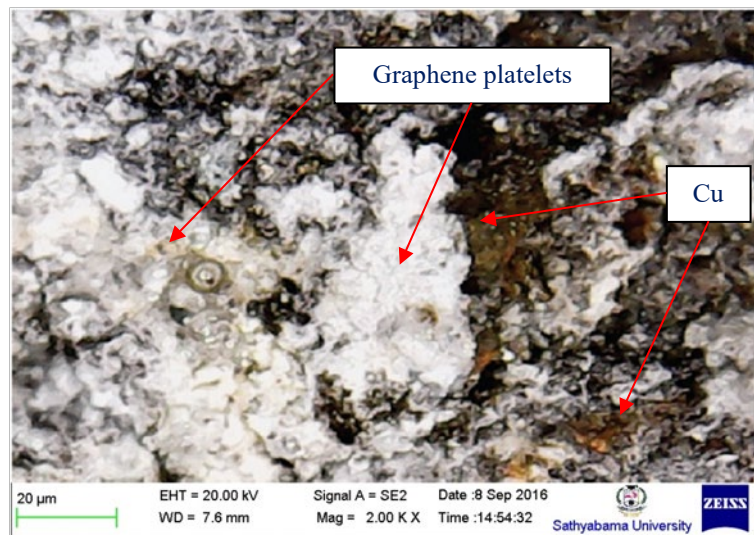


Figure 10. Graphene existence observed through SEM at the SZ of Al-Cu joint.

With the tool rotational speed of 1000 rpm in weave weld condition, the graphene platelets shifted in weave path through uniform dispersion in locating the particles (as can be observed in Figure 12(a)) along the shear plane, thereby increased the impact strength of the weldments. This confirmed with energy dispersive X-Ray analysis (EDAX) as presented in Figure 12(b). When the tool rotational speed was below 1000 rpm, the percentage of elongation in the FSW joint was minimum. The heat input induced at a tool rotational speed of 1000 rpm had a strong influence on the percentage

of elongation. At a rotational speed of 1000 rpm, the tensile strength reached a maximum value, along with an increase in the percentage of elongation. While increasing the rotational speed above 1200 rpm, the tensile strength of the joint reduced because of the advanced heat input per unit length, and a slower cooling rate in the FSW zone. This caused grain growth as can be seen in Figure 11(b), subsequently leading to a lower percentage of elongation of the joints. The elongation of the material depends on the maximum ductility and minimum formation of intermetallic compounds, which was restricted by the graphene platelets in preventing the formation of oxides for a defect-free joint.

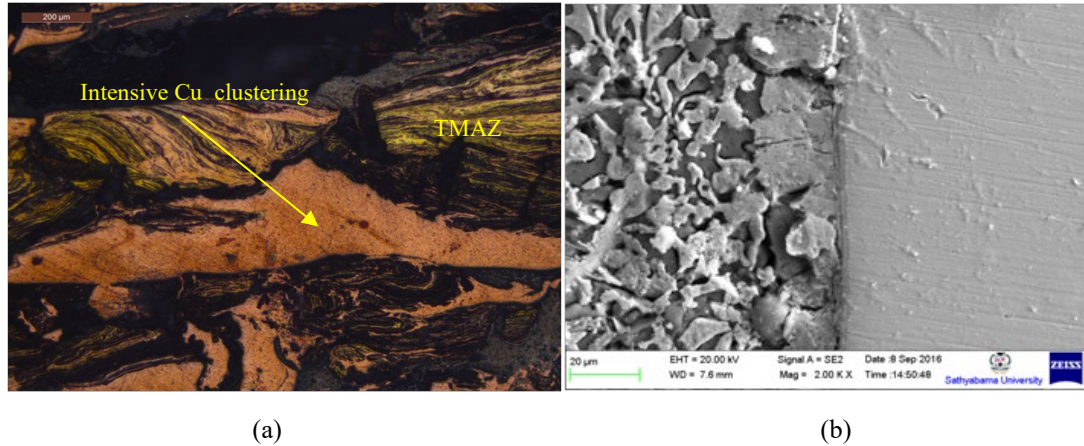


Figure 11. (a) Intensive material clustering and, (b) grain growth at stir zone.

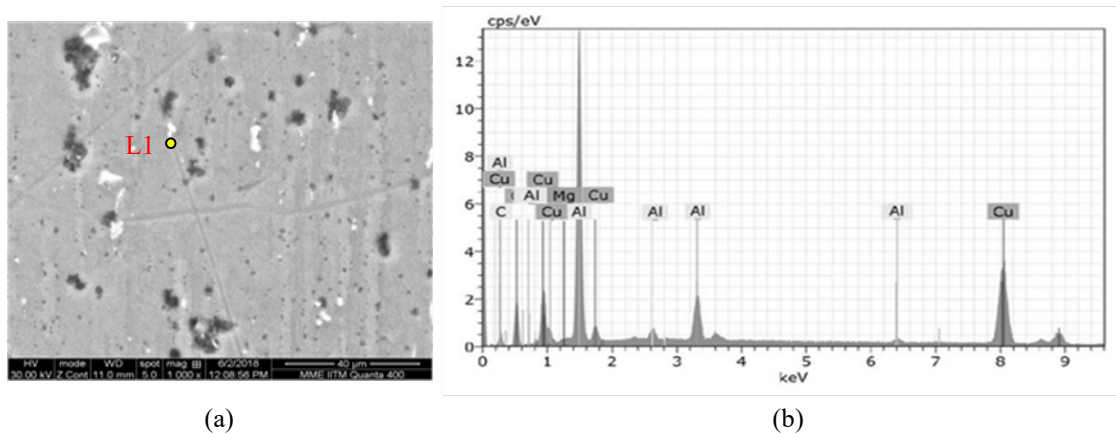


Figure 12(a). SEM image of stir zone under WW-WOPO (with GNPs) of 1000 rpm, (b) EDAX image of the stir zone: L1.

CONCLUSION

The effect of each parameter on the mechanical properties under four welding conditions, namely, LW-WOPO, LW-WPO, WW-WOPO, and WW-WPO was evaluated.

- i. The best tensile strength obtained with the effect of tool rotational speed under weave weld with pin offset condition with reinforcement was 13.82 % higher than the weld obtained under the same condition without reinforcement. This results in 77.5 % of aluminium base material strength and 96.44% of copper base material strength.
- ii. IMCs such as AlCu, Al₂Cu, and Al₄Cu₉ large size band layers were observed with the welding conditions LW-WOPO, whereas in conditions such as WW-WPO, WW- WPO resulted in the formation of the thin uniform layer. This was due to severe plastic deformation and grain refinement in the SZ based on the Zener pinning effect.
- iii. Rising dislocations and grain boundaries in the weld nugget (WN) facilitated short circuit diffusion, and thus accelerated the formation of Al₄Cu₉ and Al₂Cu phases. Moreover, Al₄Cu₉ phase was mainly distributed in the Cu/WN area, which was consistent with the intercalation patterns formed within this region. The formation of IMC Al₂C and Al₄C₃ (aluminium carbide) was found in the weld nugget for the joint made with the addition of GNPs.

ACKNOWLEDGEMENT

The authors would like to express their gratitude to Centre for Composite Fabrication and Testing, RMK College of Engineering and Technology and Centre for Materials Joining and Research, Annamalai University for providing assistance in performing the experiments.

REFERENCES

- [1] Jayabalakrishnan D, Balasubramanian M. Friction stir weave welding (FSWW) of AA6061 aluminium alloy with a novel tool path pattern. *Australian Journal of Mechanical Engineering* 2017; 17(2): 133-144.
- [2] Jayabalakrishnan D, Balasubramanian M. Friction stir welding of dissimilar butt joints with novel joint geometry. *Acta Physica Polonica A* 2018; 133: 94-100.
- [3] Ouyang J, Yarrapareddy E, Kovacevic R. Microstructural evolution in the friction stir welded 6061 aluminium alloy (T6-temper condition) to copper. *Journal of Materials Processing Technology* 2006; 172: 110-112.
- [4] Liu P, Shi QY, Wang W, Wang X, Zhang Z. Microstructure and XRD analysis of FSW joints for copper T2/aluminium 5A06 dissimilar materials. *Materials Letters* 2008; 62: 4106-4108.
- [5] Sinha VC, Kundu S, Chatterjee S. Microstructure and mechanical properties of similar and dissimilar joints of aluminium alloy and pure copper by friction stir welding. *Perspectives in Science* 2016; 8: 543-546.
- [6] Yuqing M, Liming K, Fencheng L, Qiang L, Chunping H, Li X. Effect of tool pin eccentricity on microstructure and mechanical properties in friction stir welded 7075 aluminium alloy thick plate. *Materials and Design* 2014; 62:334-343
- [7] Cabibbo, M, Forcellese, AM, Simoncini, M, Peralisi, D, Ciccarelli. Effect of welding motion and pre-/post-annealing of friction stir welded AA5754 joints. *Materials & Design* 2016; 93: 146-159.
- [8] Mehta KP, Badheka VJ. Effects of tilt angle on the properties of dissimilar friction stir welding copper to aluminium. *Materials and Manufacturing Processes* 2016; 31(3): 255-263.
- [9] Mehta KP, Badheka VJ. Hybrid approaches of assisted heating and cooling for friction stir welding of copper to aluminium joints. *Journal of Materials Processing Technology* 2017; 239: 336-345.
- [10] Galvao I, Loureiro A, Rodrigues DM. Critical review on friction stir welding of aluminium to copper. *Science and Technology of Welding and Joining* 2016;21(7): 523-546.
- [11] Selamat NFM, Baghdadi AH, Sajuri Z Kokabi AH. Friction stir welding of similar and dissimilar aluminium alloys for automotive applications. *International Journal of Automotive and Mechanical Engineering* 2016; 13(2): 3401 - 3412.
- [12] Shah LH, Midawi ARH, Walbridge S, Gerlich A. Influence of tool offsetting and base metal positioning on the material flow of AA5052-AA6061 dissimilar friction stir welding. *Journal of Mechanical Engineering and Sciences* 2020; 14(1); 6393 - 6402.
- [13] Ibrahim Sabry, El-Kassas AM. An appraisal of characteristic mechanical properties and microstructure of friction stir welding for Aluminium 6061 alloy – Silicon Carbide (SiCp) metal matrix composite. *Journal of Mechanical Engineering and Sciences* 2019; 13(4); 5804-5817.
- [14] Sathari NAA, Razali AR, Ishak M, Shah LH. Mechanical strength of dissimilar AA7075 and AA6061 aluminum alloys using friction stir welding. *International Journal of Automotive and Mechanical Engineering* 2015; 11; 2713-2721.
- [15] Li XW, Zhang DT, Qiu C, Zhang W. Microstructure and mechanical properties of dissimilar pure copper/1350 aluminium alloy butt joints by friction stir welding. *Transactions of Nonferrous Metals Society of China* 2012; 2(6):1298-1306.
- [16] Sahu PK, Kumari K, Pal S, Pal SK. Hybrid fuzzy-grey-Taguchi based multi weld quality optimisation of Al/Cu dissimilar friction stir welded joints. *Advances in Manufacturing* 2016; 4: 237-247.
- [17] Kahl S, Osikowicz W. Composite aluminium-copper sheet material by friction stir welding and cold rolling. *Journal of Materials Engineering and Performance* 2013; 22: 2176-2184
- [18] Bhattacharya T, Das H, Jana S, Pal T. Numerical and experimental investigation of thermal history, material flow, and mechanical properties of friction stir welded aluminium alloy to DHP copper dissimilar joint. *The International Journal of Advanced Manufacturing Technology* 2017; 88: 847-861.
- [19] Sahu PK, Pal S, Pal SK, Jain R. Influence of plate position, tool offset and tool rotational speed on mechanical properties and microstructures of dissimilar Al/Cu friction stir welding joints. *Journal of Materials Processing Technology* 2016; 235:55-67.
- [20] Akinlabi, ET. Effect of shoulder size on weld properties of dissimilar metal friction stir welds. *Journal of Materials Engineering and Performance* 2012; 21(7):1514-1519.
- [21] Singh, RKR, Prasad, R, Pandey, S. Mechanical properties of friction stir welded dissimilar metals. *Proceedings of the National Conference on Trends and Advances in Mechanical Engineering*, pp.579-583; 2012
- [22] Avettand-Fenoel, MN, Taillard, R, Ji, G, Goran, D. Multi scale study of interfacial intermetallic compounds in a dissimilar Al 6082-T6/Cu friction-stir weld. *Metallurgical and Materials Transactions A: Physical Metallurgy and Materials Science* 2012; 43(12):4655-4666.
- [23] Singarapu, U, Adepu, K, Arumalle, SR. Influence of tool material and rotational speed on mechanical properties of friction stir welded AZ31B magnesium alloy. *Journal of Magnesium and Alloys* 2015; 3(4): 335-344.
- [24] Jayabalakrishnan D Balasubramanian M. Eccentric-weave friction stir welding between Cu and AA 6061-T6 with reinforced graphene nanoparticles. *Materials and Manufacturing Processes* 2018; 33(3):333-342.
- [25] Mehta, KP, Badheka, VJ. A review on dissimilar friction stir welding of copper to aluminium: process, properties, and variants. *Materials and Manufacturing Processes* 2015; 31(3): 233-254.
- [26] Al-Jarrah, JA. Surface morphology and mechanical properties of aluminium-copper joints welded by friction stir welding. *Jordan Contemporary Engineering Sciences* 2014; 7(5): 219 - 230.